Effects of bulk dissipation on the critical exponents of a sandpile

Chai-Yu Lin,[1,2,*] Chien-Fu Chen,[1] Chi-Ning Chen,[3] Chao-Shun Yang,[4] and I-Min Jiang[4]
[1]*Department of Physics, National Chung Cheng University, Chia-Yi 66117, Taiwan*
[2]*National Center for Theoretical Sciences at Taipei, Physics Division, National Taiwan University, Taipei 10617, Taiwan*
[3]*Department of Physics, National Dong Hwa University, Hualien 97441, Taiwan*
[4]*Department of Physics, National Sun Yat-Sen University, Kaohsiung 80424, Taiwan*
(Received 6 May 2004; revised manuscript received 18 March 2006; published 18 September 2006)

Bulk dissipation of a sandpile on a square lattice with the periodic boundary condition is investigated through a dissipating probability f during each toppling process. We find that the power-law behavior is broken for $f>10^{-1}$ and not evident for $10^{-1}>f>10^{-2}$. In the range $10^{-2}\geq f\geq 10^{-5}$, numerical simulations for the toppling size exponents of all, dissipative, and last waves have been studied. Two kinds of definitions for exponents are considered: the exponents obtained from the direct fitting of data and the exponents defined by the simple scaling. Our result shows that the exponents from these two definitions may be different. Furthermore, we propose analytic expressions of the exponents for the direct fitting, and it is consistent with the numerical result. Finally, we point out that small dissipation drives the behavior of this model toward the simple scaling.

DOI: 10.1103/PhysRevE.74.031304 PACS number(s): 45.70.Ht, 05.65.+b, 64.60.Ak

I. INTRODUCTION

Self-organized criticality (SOC) [1] as proposed by Bak, Tang, and Wiesenfeld (BTW) provides a possible pathway to understand the underlying mechanism of scaling behaviors [2] in many natural phenomena [3]. The SOC models, which automatically exhibit power-law behavior, are nonequilibrium systems with very few exact solutions. If we use the traditional phase transition [4] to understand SOC, the source problem of SOC is still a challenge, i.e., why a system without tuning any parameters can arrive at the critical state with power-law behavior. Basically, a SOC system is maintained by a feedback mechanism that repeatedly receives energy in a random fashion and dissipates energy in a specific way. In a steady state, the input flow equals the dissipative flow on average. In general, the dissipation is either through the boundary or bulk. The BTW sandpile [1], Manna sandpile [5], Olso rice pile model [6], etc., are prototypical for boundary dissipation, whereas the OFC earthquake [7] and the fixed energy sandpile [8,9] involve bulk dissipation. In SOC, the dissipation always plays important roles, e.g., determining the scaling behavior [10] in the BTW sandpile model, destroying the universality class or criticality in the OFC model [7], fixing the total energy to discuss the source of SOC [8,9], etc. Both the source and critical exponents problems reveal how dissipations lead to a much better understanding of SOC.

The BTW sandpile model [1] was the first SOC model and built by boundary dissipation. In this model, the distributions of avalanche sizes were originally expected to exhibit power-law behavior. However, Refs. [11,12] showed that the avalanche size distributions may follow multifractal scaling. The determination of the avalanche exponents thus requires a more detailed analysis of the relaxation process. One way for approaching this goal is to represent the whole avalanche as a series of more elementary events and then express the avalanche exponents through the exponents of these elementary events. Such an approach was first introduced by Dhar and Manna [13]. They performed a procedure to decompose an avalanche into a series of elementary events called inverse avalanches. Later, the wave of topplings [14] were also successful in decomposing an avalanche through a rearrangement of the toppling order. It has been showed that both inverse avalanches and waves would lead to the same representation [14]. Unlike avalanches, the wave of topplings is not a standard observation of a sandpile and difficult to relate to any real dynamics for SOC. However, Priezzhev *et al.* established scaling relations between the wave and avalanche exponents [15]. The avalanche exponents thus can be expressed by the wave exponents which makes the usage of waves effective. Based on the above statement and the investigation [16] in which waves have a clearer scaling form than avalanches, the wave of topplings is a useful tool for understanding the behavior of a sandpile.

Compared with boundary dissipation, bulk dissipation is seldom considered. In this paper, we investigate bulk dissipation for a sandpile. Here, we use a modified version of the BTW sandpile model, called the dissipative toppling (DT) model, to investigate the effects of bulk dissipation. In the DT model, a parameter f is used to control bulk dissipation while the basic essence of the BTW sandpile is kept. The reasons for choosing such a BTW-like model are as follows: (i) The BTW sandpile has satisfactory theoretical results [17–19], which could be a basis for our DT model. (ii) Both the DT model and the fixed energy sandpile [8] are built on a lattice with the periodic boundary condition. The fixed energy sandpile can also be considered as a BTW-like model but its bulk dissipation is different from that of the DT model. The scaling correction effect of the fixed energy sandpile was turned out to be effectively reduced because of the possibility of using periodic boundary condition [8]. The roles of dissipating way and boundary condition in scaling behavior may be revealed further by studying the DT model. (iii) The toppling rule of the DT sandpile is different from

*Electronic address: lincy@phy.ccu.edu.tw

that of the OFC model. Our result for the influence of bulk dissipation on the exponents can be compared with that of the OFC model.

From the above three points, applying the wave concept to the DT sandpile with bulk dissipation may be a worthwhile effort in understanding the source and scaling behavior of SOC. This paper is organized as follows. In Sec. II, we establish the validness of the wave representation of the DT sandpile. In Sec. III, the wave exponents defined by both direct measurement and the simple scaling are obtained from numerical simulations. The analysis of direct measurement exponents for the wave are shown in Sec. IV. It is found that the values of the exponents and equality among exponents from simulations are consistent with analytic expressions. Finally, we have a summary in Sec. V.

II. DISSIPATIVE TOPPLINGS SANDPILE MODEL

The original BTW sandpile is established on a $L\times L$ square lattice (L^2 sites). Every lattice site is labeled by an integer i and assigned a positive integer z_i as its height, where $1\leq i\leq L^2$. The height configuration of these L^2 sites $\mathcal{C}=\{z_i\}$ characterizes the status of the sandpile. The critical value $z^c=4$ is the threshold of the sandpile toppling. There are two conditions for a specified site j with height z_j. When $z_j>z^c$, site j is unstable and a dynamic process will take place. This process called a toppling involves the grain exchange between site j and its four nearest neighbor (NN) sites. The toppling rule is that site j sends four grains to its NN sites and each NN site receives one grain. The mathematical formula is expressed as

$$z_j \to z_j - 4,$$

$$z_{j_k} \to z_{j_k} + 1, \tag{1}$$

where site j_k is the kth NN site of site j for $k=1$, 2, 3, and 4. On the other hand, when $z_j\leq z^c$, site j is stable and z_j will remain unchanged, i.e., there is no dynamic process.

In the beginning of the sandpile evolution, the height z_i is restricted to $1\leq z_i\leq z^c$. At first, one grain falls on a randomly chosen lattice site called the initial site I. The height of this initial site then increases by 1 ($z_I\to z_I+1$). If $z_I>z^c$, it triggers a series of topplings where every unstable site topples through Eq. (1). The heights finally arrive at a configuration $\{z_i\}$ with $z_i\leq z^c$ for all i. This relaxation process, called an avalanche, consists of a set of topplings. During an avalanche, each site can topple many times and different sites can topple different times. Therefore, an avalanche can be marked by two toppling sizes: (i) the total number of topplings n_{ava} and (ii) the toppling area which is the number of distinct sites toppled s_{ava}. Usually, this model is built on the open boundary condition. That is to say, grains are allowed to leave the system through the boundary.

After all lattice sites are stable, we repeat the sandpile procedure by adding a grain to the system (I is reassigned a new value for each adding procedure). Continuing this adding and toppling processes many times and then measuring the probability distribution function of an avalanche size, for example, n_{ava}, we expect $P(n_{\mathrm{ava}})\sim n_{\mathrm{ava}}^{-\tau_{n_{\mathrm{ava}}}}$, where $P(n_{\mathrm{ava}})$ and $\tau_{n_{\mathrm{ava}}}$ are the probability distribution and the exponent of toppling number for avalanches, respectively.

The BTW sandpile dissipates grains through the boundary. If the BTW model is built on a $L\times L$ square lattice with the periodic boundary condition, there is no loss and the added grains will stay in the system. Consequently, it will lead to an infinite n_{ava} for a finite system, i.e., the toppling process cannot stop. This result renders us unable to do the adding procedure for the next stage because the system cannot arrive at a stable height configuration. In our study, we consider a BTW-like sandpile with dissipations during each toppling process. We call this model the dissipative topplings (DT) sandpile model. There is a dissipating probability f such that one specific NN site j_k of an unstable site j does not receive a grain during the toppling process of site j. The toppling rule of the DT model is expressed as

$$z_j \to z_j - 4,$$

$$z_{j_k} \to \begin{cases} z_{j_k} & \text{with probability } f, \\ z_{j_k}+1 & \text{with probability } 1-f, \end{cases} \tag{2}$$

where $z_{j_k}\to z_{j_k}$ and $z_{j_k}\to z_{j_k}+1$ correspond to a dissipative dynamics and a conservative (nondissipative) dynamics, respectively. Note that our DT model is built on a lattice with the periodic boundary condition. No grain can leave through the boundary. The bulk dissipation of the DT model is different from that of the fixed energy sandpile model [8] which also possesses the periodic boundary condition. The fixed energy sandpile dissipates one grain after one avalanche finishes. There are two ways for dissipating a grain. (i) Random subtract. A random site is chosen to lose one grain. (ii) Continuous subtract: Every site i loses grains. The lost grain number of each site is proportional to the local height and the total number of the lost grain is exact one. On the other hand, the DT dissipates unrestraint units of grain during the topplings of an avalanche through Eq. (2).

The operators for sandpile a_l and b_l denote that a grain is subtracted from and added to site l, respectively. They are expressed as

$$a_l{:}z_l \to z_l - 1,$$

$$b_l{:}z_l \to z_l + 1. \tag{3}$$

For example, m grains are subtracted from site l ($z_l\to z_l-m$) and added to site l ($z_l\to z_l+m$) correspond to $(a_l)^m$ and $(b_l)^m$, respectively. In Eq. (2), $z_j\to z_j-4$, $z_{j_k}\to z_{j_k}$ and $z_{j_k}\to z_{j_k}+1$ are expressed as $(a_j)^4$, $(b_{j_k})^0$, and $(b_{j_k})^1$, respectively. The toppling rule of site j in the DT sandpile thus can be characterized by the operator $A_j(Q)=a_j^4(b_{j_1})^{q_1}(b_{j_2})^{q_2}(b_{j_3})^{q_3}(b_{j_4})^{q_4}$, where $Q=(q_1,q_2,q_3,q_4)$ and $q_k=0$ or 1. From Eq. (2), the probability of site j having the toppling rule with parameter Q, prob$[A_j(Q)]$, is

$$\text{prob}[A_j(Q)] = \prod_{k=1}^{4} [f^{\delta(0,q_k)}][(1-f)^{\delta(1,q_k)}], \tag{4}$$

where δ is the Kronecker-Delta function. For example, site j with the toppling rule of the BTW shown in Eq. (1) corresponds to $Q=(q_1,q_2,q_3,q_4)=(1,1,1,1)$. The probability of such a toppling rule is $(1-f)^4$. Note that the Eq. (4) is applied at every toppling process. It is not picked once for every site at the beginning of the simulation. Generally speaking, there are 2^4 kinds of toppling rules in the DT model.

Consider $\mathcal{C}_0$ as an intermediate height configuration which possesses unstable sites v_1, v_2,…, etc. We use $\{v_r\}_{\mathcal{C}_0}$ to represent the set of unstable sites, where r is the label of the unstable sites. The system will topple and then finally arrive at a stable height configuration $\mathcal{C}_f$. Different toppling order for these unstable sites of $\mathcal{C}_0$ will result in the same $\mathcal{C}_f$. This inference can be explained by the topplings of any two of unstable sites. If sites α and β are two of the unstable sites of $\mathcal{C}_0$ with α and $\beta \in \{v_r\}_{\mathcal{C}_0}$, the height should satisfy $z_\alpha > z^c$ and $z_\beta > z^c$. These two sites topple through their toppling operators $A_\alpha(Q_\alpha)$ and $A_\beta(Q_\beta)$, respectively, where Q_α and Q_β are two specified choices of Q. If we let site β topple first and then let site α topple, the height configuration becomes $\mathcal{C}'=A_\alpha(Q_\alpha)A_\beta(Q_\beta)\mathcal{C}_0$. It is obvious that $\mathcal{C}'=A_\alpha(Q_\alpha)A_\beta(Q_\beta)\mathcal{C}_0 = A_\beta(Q_\beta)A_\alpha(Q_\alpha)\mathcal{C}_0$. Therefore, changing the toppling order of unstable sites for an intermediate height will result in the same configuration $\mathcal{C}_f$.

Suppose that $\alpha \in \{v_r\}_{\mathcal{C}_0}$. If we topple all unstable sites of $\mathcal{C}_0$ except site α (i.e., $\{v_r\}_{\mathcal{C}_0} - \{\alpha\}$), the system arrives at another intermediate height $\mathcal{C}_1$ which has unstable site set $\{v_r\}_{\mathcal{C}_1}$ with $\alpha \in \{v_r\}_{\mathcal{C}_1}$. Changing the toppling order for $\mathcal{C}_1$ will not affect the final height $\mathcal{C}_f$. Now, we still topple all unstable sites of $\mathcal{C}_1$ except site α ($\{v_r\}_{\mathcal{C}_1} - \{\alpha\}$)and then arrive at $\mathcal{C}_2$ with unstable site set $\{v_r\}_{\mathcal{C}_2}$ with $\alpha \in \{v_r\}_{\mathcal{C}_2}$. Continue this process for T times. If $\mathcal{C}_T$ has only one unstable site α ($\{v_r\}_{\mathcal{C}_T}=\{\alpha\}$), we call this way of topplings from $\mathcal{C}_0$ to $\mathcal{C}_T$ "the freezing procedure" of site α. This procedure, which involves the changing of the toppling order of unstable sites for each stage of an intermediate configuration, will not change the final configuration $\mathcal{C}_f$.

Consider the following process of topplings called "wave of topplings." If the initial site I to which a grain was added becomes unstable, topple it once, and then topple all other sites of the lattice that become unstable. During this process, we must keep the initial site I from a second toppling [20]. That is to say, we do the freezing procedure for $\alpha=I$. The set of sites toppled is called "the first wave." After the first wave is completed, site I is then allowed to topple the second time, and is not permitted to topple again (i.e., do the freezing procedure with $\alpha=I$) until the second wave is finished. This process continues and generates the third, fourth,…,waves. After the topplings of the ηth wave, site I finally becomes stable. We call the ηth wave "the last wave." Through the above procedure, the topplings of a series of waves just rearrange the toppling order of an avalanche. An avalanche can be decomposed into a series of waves.

A stable sandpile system with height $z_i=h(i)$ is triggered by adding one grain to site I, where $1 \le h(i) \le 4$. During an avalanche, the received grain number from adding process is $N_0(i)$, where $N_0(i)=1$ for $i=I$ and $N_0(i)=0$ for $i \neq I$. Suppose site j, which has received $M^{(t)}(j_k,j)$ grains from its kth NN site, is ready to experience the tth toppling. We have

$$N_0(j) + N_1^{(t)}(j) + h(j) - 4t \ge 1, \tag{5}$$

where $N_1^{(t)}(j)=M^{(t)}(j_1,j)+M^{(t)}(j_2,j)+M^{(t)}(j_3,j)+M^{(t)}(j_4,j)$ is the received grain number for site j from its NN sites and $4t$ is the lost grain number for site j after its tth toppling. In the DT model, due to the bulk dissipation, $M^{(t)}(j_k,j)$ is smaller than or equal to the toppling number of site j_k.

Consider that the sites IA, IB,…, are the leading sites of $t=2$ which means these sites can first finish the second toppling. That is to say, sites IA, IB,…, topple twice simultaneously and at the same time other sites cannot topple the second time. Before this time that site IA topples the second time, all sites of system have toppled at most once. If site IA_k is the NN site of site IA, we have $N_1^{(2)}(IA)=M^{(2)}(IA_1,IA)+M^{(2)}(IA_2,IA)+M^{(2)}(IA_3,IA)+M^{(2)}(IA_4,IA)$. Then, $N_1^{(t=2)}(IA) \le 4$ because $0 \le M^{(t=2)}(IA_k,IA) \le 1$. After receiving $N_0(IA)+N_1^{(2)}(IA)$ grains, site IA should be ready to satisfy Eq. (5) with $t=2$. From Eq. (5), $N_0(IA) \ge 1-N_1^{(2)}(IA)-h(IA)+8 \ge 1$ must hold. However, $N_0(IA) \ge 1$ only holds for $IA=I$. We conclude that there is only one leading site of $t=2$ and this site is the initial site I. Therefore, if site I is not allowed to topple twice, every site topples at most once. From the definition of the first wave, any toppling site topples exactly once for the first wave.

After the first wave is finished, the height configuration arrives at $z_j=z_j^* \le 4$ for $j \neq I$ and $z_j=z_j^*=5$ for $j=I$ (if the second wave exists). This situation is exactly the same as a system, with the stable height $h(j)=z_j^*$ for $j \neq I$ and $h(j)=z_j^*-1$ for $j=I$, is added a grain to site I. Now, a new avalanche happens in this system. If we use the Eq. (5) with $t=2$ to this new avalanche again, the toppling sites of the first wave of this new avalanche topples exactly once. However, the first wave of this new avalanche is the second wave of the original avalanche. Continuing this same argument for the third, the fourth,…, waves, we can conclude that any toppling site topples exactly once for a wave [14].

In general, an avalanche must be marked by the toppling area s_{ava} and the toppling number n_{ava}. The toppling area and the toppling number of a wave are denoted by s and n, respectively. Based on the above discussion, however, a wave can be simply characterized only by the toppling area s ($s=n$ for a wave). This feature along with the better scaling gives the reasons why we use waves but not avalanches for characterizing sandpiles in this study [21].

In this work, in order to study the effects of bulk dissipation on a sandpile system, we calculate the probability distribution functions for three categories of waves. (i) All waves: This is the general feature of sandpile dynamics. Here, every toppling site topples through one of 16 kinds of toppling rules. (ii) Dissipative waves: It describes the role of dissipation. The definition is given by a wave containing at least one dissipative toppling which corresponds to the rule

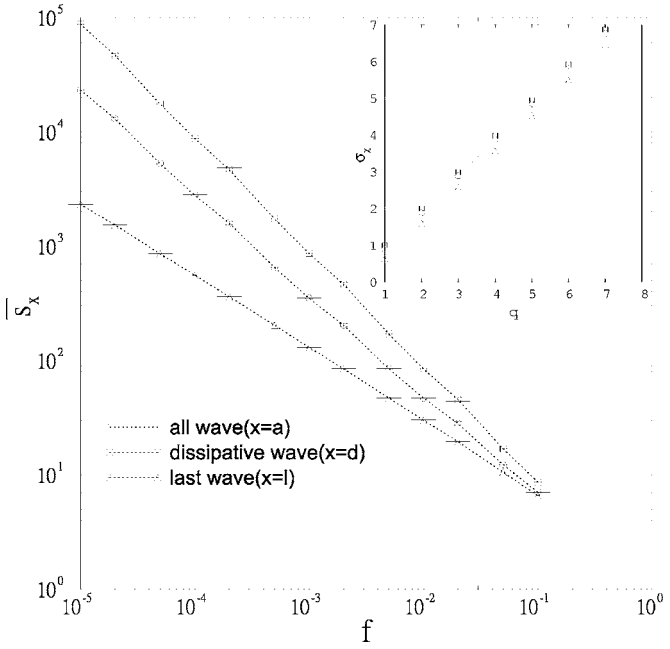

FIG. 1. Mean toppling sizes $\bar{s}_x$ as a function of f for all waves $x=a$ (○), dissipative waves $x=d$ (□), and last waves $x=d$ (△). The slopes for s_a, s_d, and s_l are −0.89, −1.00, and −0.63, respectively. In the inset, we show σ_x as a function of q.

$z_{j_k} \to z_{j_k}$ of Eq. (2). That is to say, a dissipative toppling has a toppling parameter of $Q=(q_1,q_2,q_3,q_4)$ with constraint $\Pi_{k=1}^{4} q_k=0$. There are 15 kinds of toppling rules for a dissipative toppling. (iii) Last waves: The end of topplings, which refers to the last waves, is due to two mechanisms, grain redistribution and dissipation. Therefore, the last wave is an auxiliary index for the effects of dissipation.

III. NUMERICAL RESULTS

Our simulations for the DT model are on a $L \times L$ square lattice for $L=1000$ with the periodic boundary condition, which assures that the grain dissipation is only through bulk dissipation. 5×10^6 grains are randomly added for each $f = a \times 10^{-b}$ with the constraint $f \leq 0.1$, where $a=1$, 2, and 5 and $b=2$, 3, 4, and 5. In order to sample the data of the critical states, we take the data of the latter 4×10^6 grains. When one grain is added to an initial site I with $z_I=4$, z_I becomes 5. Site I will trigger a series of topplings with toppling number n_{ava}. The expected number of dissipated grains is $4n_{\text{ava}}f$, which can be realized from Eq. (2). In the steady state, the average number of added grains is equal to that of dissipated grains. Extending this statement to one avalanche process, we expect that the mean toppled number $\bar{n}_{\text{ava}}$ for an avalanche satisfies $(\text{prob}[z_I=4])(4\bar{n}_{\text{ava}}f)=1$, where $\text{prob}[z_I=4]$ is the probability of z_I being 4. That is $\bar{n}_{\text{ava}} \sim f^{-1}$ since $\text{prob}[z_I=4]$ is a constant when the system has reached the steady state.

Now we turn to the wave where $s=n$. In general, the mean toppling area $\bar{s}_x$ is related to the lattice size L and the dissipating probability f, where $x=a$ (all waves), d (dissipative waves), and l (last waves). In Fig. 1, we show the mean toppling area $\bar{s}_x$ as a function of f for $x=a$, d, and l. It is worth noting that $s_d \sim f^{-1}$, $s_a \sim f^{-0.89}$, and $s_l \sim f^{-0.63}$. There is no grain added for successive waves during an avalanche. Unlike the case of the avalanche, we cannot conjecture $\bar{s}_x \sim f^{-1}$ for a wave. However, $\bar{s}_d$ for a wave has the same function form as $\bar{n}_{\text{ava}}$ for an avalanche. It reveals that dissipative waves should play a pivotal role in the dynamics of the DT model. In the BTW sandpile on a $L \times L$ lattice with the open boundary condition, grain dissipation is only through the boundary. Therefore, we expect the $\bar{s}_x$ is a function of L. If a DT model is built on a lattice with the open boundary, grains can leave the system by both boundary and bulk dissipations. Again, we can expect that $\bar{s}_x=\bar{s}_x(L,f)$. Our DT model is built by the periodic boundary condition which reduces the effect of L on $\bar{s}_x$. Furthermore, if $\bar{s}_x \ll L^2$, the finite size effect (L) is overshadowed by the effect of the bulk dissipation effect (f). We expect that $\bar{s}_x=\bar{s}_x(f)$ [22]. In the case $L=1000$, we find that $\bar{s}_x \ll L^2$ for $f \geq 10^{-5}$ shown in Fig. 1. Therefore, we expect that $\bar{s}_x=\bar{s}_x(f)$ for $f \geq 10^{-5}$.

To determine the critical exponents, we first calculate the probability distributions function $P_x(s,f)$ as a function of s at $f=10^{-1}$, 10^{-2}, and 10^{-5}, where $x=a,d$, and l. In general, the probability distribution function in a critical system should consist mainly of two parts: a power-law decay (the main body) and an exponential decay (the tail). Usually, the power-law decay only holds in a range $[s_{m1},s_{m2}]$, where s_{m1} and s_{m2} are the lower and upper cutoffs, respectively. In general, s_{m1} is the order of lattice constant and s_{m2} can be considered as the border between power-law decay and exponential decay. In order to determine the asymptotic behavior of $P_x(s,f)$, we define the direct measurement for an exponent as the following form:

$$P_x(s,f) = \begin{cases} c_x s^{-\omega_x} & \text{for } s_{m1} \leq s \leq s_{m2}, \\ \theta(s,f) & \text{for } s > s_{m2}, \end{cases} \tag{6}$$

where ω_x is the exponent of the direct measurement, $c_x(f)$ is independent of s, and $\theta(s,f)$ varies as or faster than an exponential decay for a fixed f. In Fig. 2, it is evident that the power-law behaviors are valid, except in the case $f=10^{-1}$ which is dominated by the tail. Therefore, two constraints in our simulations, which keep the clearer power-law behaviors, should be noted: (i) $f \leq 10^{-2}$. If $f > 10^{-2}$, the $\bar{s}_x$ or $[s_{m1},s_{m2}]$ is too small, i.e., the power-law behavior is not obvious. (ii) $f \geq 10^{-5}$. $\bar{s}_x$, s_{m2}, and ω_x will depend on both L and f. However, if we restrict that $\bar{s}_x \ll L^2$ [22], $s_{m2}=s_{m2}(f)$ and $\omega_x=\omega_x(f)$ will not depend on L. In this paper, because we only focus on bulk dissipation, we have such constraints listed in (i) and (ii). If we take a larger L, f is allowed to be much smaller.

If $P_x(s,f)$ satisfies the standard form of the simple scaling, both power-law and tail parts of Eq. (6) can be described by the following form:

$$P_x(s,f) = s^{-\tau_x} G_x(sf^{D_x}) = f^{\tau_x D_x} G_x'(sf^{D_x}) \quad \text{for } f < f_x^c, \tag{7}$$

where f_x^c (depends on the microscopic details of the model) is an index for the correction of simple scaling [23], $\tau_x \geq 1$ [24] and D_x are two independent critical exponents $G_x(u)$ and $G_x'(u)$ are the scaling functions with $u=sf^{D_x}$. In order to dis-

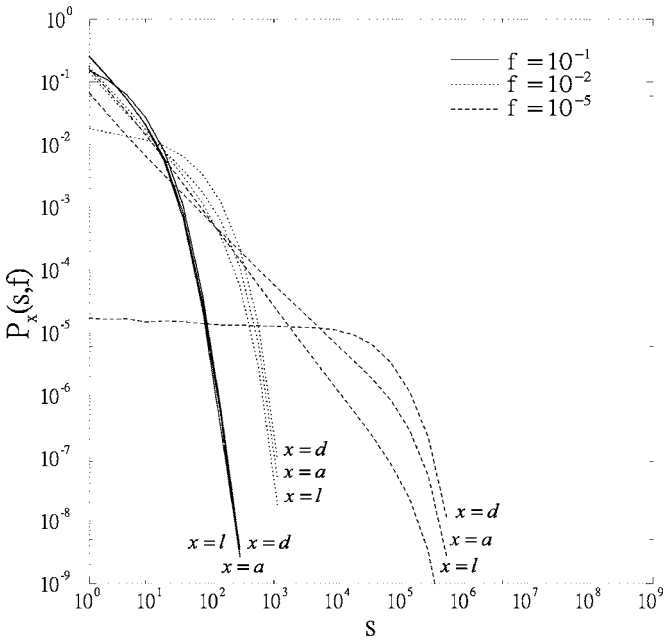

FIG. 2. The probability distribution $P_x(s,f)$ for $f=10^{-1}$ (solid lines), 10^{-2} (dotted lines), and 10^{-5} (dash lines), where $x=a$, d, and l represent all waves, dissipative waves, and last waves, respectively.

tinguish between ω_x and τ_x for the work in this paper, we specifically consider two scaling functions in the power-law region by the following form:

$$G_x(u) \sim u^{-\Delta_x},$$

$$G'_x(u) \sim u^{-\delta_x} \quad \text{for } s_{m1}f^{D_x} \le u = sf^{D_x} \le s_{m2}f^{D_x}, \tag{8}$$

where Δ_x and δ_x are two exponents. From the comparison among Eqs. (6)–(8), we have that $\Delta_x=\delta_x-\tau_x$ and $\delta_x=\omega_x$. Since τ_x, D_x, Δ_x, and δ_x are constants, it also implies that $\omega_x(f)$ for $f<f_x^c$ should be nearly a constant. The condition that $\tau_x=\omega_x$ [25] will hold only for the case $G_x(u)$ with $\Delta_x=0$ and $f<f_x^c$. Through a direct calculation, the qth moment of P_x will satisfy that

$$\overline{s_x^q} = \int s^q P_x(s,f)ds = f^{-D_x(q-\tau_x+1)} \int u^{q-\tau_x} G_x(u)du \sim f^{-\sigma_x(q)}, \tag{9}$$

where $\sigma_x(q)=D_x(q-\tau_x+1)$ for $q>\tau_x-1$ [12]. In the Fig. 1, we have already obtained that $\sigma_x(1)$ corresponds to 0.89 ($\overline{s_a}$), 1.00 ($\overline{s_d}$), and 0.63 ($\overline{s_l}$) for $x=a$, d, and l, respectively. In the inset of Fig. 1, we show the values of $\sigma_x(q)$ from $q=1$ to 7. We find the slopes of σ_x as a function of q are all 1 for $x=a$, d, and l. Therefore, if P_x satisfies Eq. (7), we have $D_x=1$ for $x=a$, d, and l. Furthermore, the simple scaling form of Eq. (7) can also be described by another two exponents $\sigma_x(1)$ and D_x as

$$P_x(s,f) = f^{2D_x-\sigma_x(1)}G'_x(sf^{D_x}). \tag{10}$$

Finally, the universality class is determined by the critical exponents τ_x and D_x. On the other hand, if $P_x(s,f)$ satisfies the multifractal scaling form [26], the universality class cannot be described by a finite set of exponents. There is no such an expression $\sigma_x(q)=D_x(q-\tau_x+1)$ for constants D_x and τ_x [12].

Another important issue about the simple scaling is the scaling correction [23,27]. Such a problem arises from the fact that Eq. (7) considers only the dominant exponents. Considering the subdominant exponents which will appear obviously for a large f, we should have corrections to Eq. (7). In other words, there exists a fixed number f_x^c such that $P_x(s,f)$ satisfies Eq. (7) for $f<f_x^c$ and deviates from Eq. (7) for $f>f_x^c$. In our model, we can expect $\omega_x(f)$ is nearly a constant for $f<f_x^c$, but not a constant for $f>f_x^c$. The determination of f_x^c needs more assumptions on the scaling behavior, e.g., the consideration in Ref. [23].

In Fig. 3(a), we show the probability distribution of all waves $P_a(s,f)$ as a function of s for $f=10^{-2}$, 10^{-3}, 10^{-4}, and 10^{-5}. We also plot $P_a(s,f)$ as a function of sf in the inset of Fig. 3(a). For each curve, we find a power-law main body, i.e., $P_a(s,f)\sim s^{-\omega_a(f)}$, where $\omega_a(f)$ is the wave size exponent of all waves for direct measurement. In Fig. 3(a), we fit the power-law behavior in the s axis from $s=s_{f1}$ to $s=s_{f2}$. The fitting intervals $[s_{f1},s_{f2}]$ are taken by $[2^2,2^6]$, $[2^2,2^9]$, $[2^2,2^{13}]$, and $[2^2,2^{16}]$ for $f=10^{-2}$, 10^{-3}, 10^{-4}, and 10^{-5}, respectively. We find that $\omega_a(f)=1$ for each f, i.e., it is independent of f within error bars. In addition, this value is identical to the value of $\omega_a=1$ [28] in the BTW sandpile.

If $P_a(s,f)$ satisfies the simple scaling with expression $\sigma_a(q)=D_a(q-\tau_a+1)$, such a simple scaling has $\sigma_a(1)=0.89$ and $D_a=1$ shown in the inset of Fig. 1. It leads to $\tau_a=2-\sigma_a(1)/D_a=1.11$. Using Eq. (10) to plot $G'_a(sf^{D_x})=f^{\sigma_a(1)-2D_a}P_a(s,f)=f^{-1.11}P_a(s,f)$ as a function of $sf^{D_a}=sf$ in Fig. 3(b), we find that these four curves are nicely collapsed, i.e., $G'_a(u)$ may exist. It also shows that $G'_a(u)\sim u^{-1.0}=u^{-\delta_a}$, i.e., $\delta_a=\omega_a=1$. For another scaling function, we plot $s^{\tau_a}P_a(s,f)=s^{1.11}P_a(s,f)=G_a(u)$ as a function of $u=sf$ in Fig. 3(c). We find that $G_a(u)\sim u^{-\Delta_a}$ with $\Delta_a=-0.11$ which confirms that $\Delta_a=\delta_a-\tau_a$. In Table I, we list the values for D_a, τ_a, Δ_a, and δ_a.

In Fig. 3(a), we expect s_{m1} is a constant for every f. Furthermore, we observe that $s_{m2}f$ is a constant, which is verified in Fig. 3(b) or the inset of Fig. 3(a). Therefore, $[s_{m1},s_{m2}]=[k_{a1},k_{a2}/f]$, where k_{a1} and k_{a2} are constants. From the definitions of $[s_{m1},s_{m2}]$ and $[s_{f1},s_{f2}]$, the fitting range $[s_{f1},s_{f2}]$ should be as close as $[s_{m1},s_{m2}]$. In our fitting, $[s_{f1},s_{f2}]$ satisfies $s_{f1}=k_{a1}$ but does not satisfy $s_{f2}=k_{a2}/f$ for each f. The reason is that we have only the data for $s=2^r$ where r is a non-negative integer. However, taking $k_{a1}=4$ and $k_{a2}=0.64$, in the sense of a log-log plot, we obtain $[\ln(s_{f1}),\ln(s_{f2})]\approx[\ln(s_{m1}),\ln(s_{m2})]$ for each f.

In Fig. 4(a), we show the probability distribution of dissipative waves $P_d(s,f)$ as a function of sf. The fitting interval $[s_{f1},s_{f2}]$ of the power-law behavior $P_d(s,f)\sim s^{-\omega_d(f)}$ is for calculating ω_d from s_{f1} to s_{f2}. We choose $[s_{f1},s_{f2}]=[2^2,2^5]$, $[2^2,2^8]$, $[2^2,2^{12}]$, and $[2^2,2^{15}]$ for $f=10^{-2}$, 10^{-3}, 10^{-4}, and 10^{-5}, respectively. Contrary to ω_a, ω_d has different values for different values of f. We find $\omega_d=0.24$, 0.13, 0.07, and 0.04 for $f=10^{-2}$, 10^{-3}, 10^{-4}, and 10^{-5}, respectively. The depen-

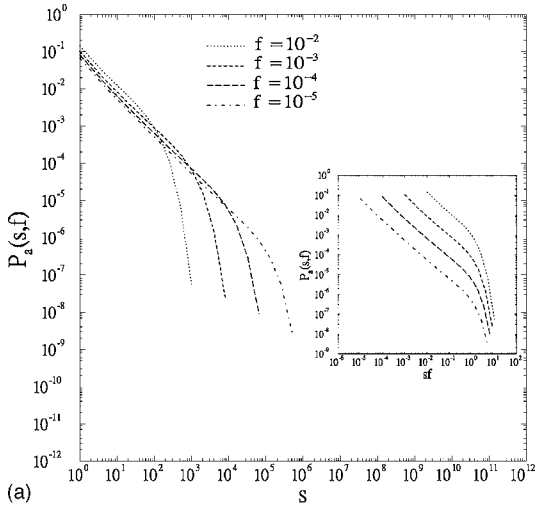

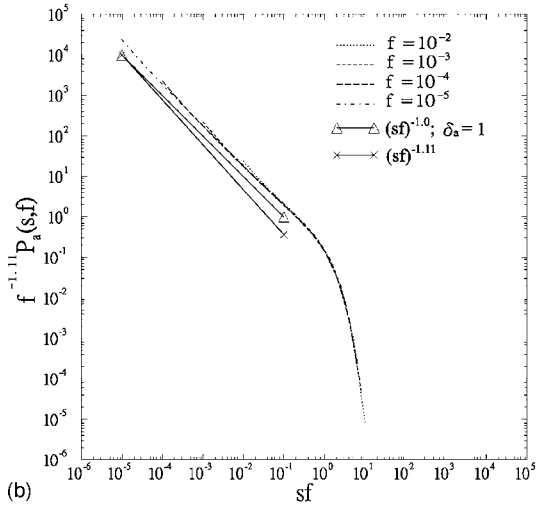

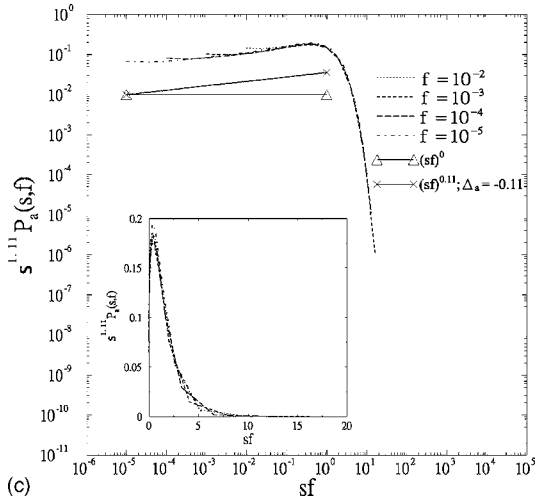

FIG. 3. (a) The probability distribution for all waves $P_a(s,f)$ as a function of s for $f=10^{-2}$ (dotted line), 10^{-3} (dash line), 10^{-4} (long dash line), and 10^{-5} (dotted dash line). $P_a(s,f)$ as a function of sf is also shown in the inset. (b) $f^{-1.11}P_a(s,f)$ as a function of sf for the data from (a). Here, we expect that $\delta_a=1$. (c) The log-log plot of $s^{1.11}P_a(s,f)$ as a function of sf for the data from (a). Here, we expect that $\Delta_a=-0.11$. The inset shows the same function in the original scale.

TABLE I. The predicted critical exponents τ_x, D_x, Δ_x, and δ_x for the simple scalings.

	τ_x	D_x	Δ_x	δ_x
$x=a$	1.11	1.00	−0.11	1.00
$x=d$	1.00	1.00	−1.00	0.00
$x=l$	1.37	1.00	0.005	1.375

dence between ω_d and f shows that $\omega_d(f)$ is a monotonically increasing function.

From the data of the inset of Fig. 1, if $P_d(s,f)$ satisfies simple scaling with $\sigma_d(q)=D_d(q-\tau_d+1)$, we have $\sigma_d(1)=1$, $D_d=1$, and $\tau_d=1$. Using the scaling form of Eq. (10), we plot $f^{\sigma_d(1)-2D_d}P_d(s,f)=f^{-1}P_d$ as a function of $u=sf$ shown in Fig. 4(b). We find that the tail parts of $f^{-1}P_d$ for various f nicely collapse together but the power-law parts do not work so nicely. The reason is that ω_d is not a constant for $f^{-1}P_d \sim (sf)^{-\omega_d}$. It also implies that the consideration of the correction to scaling is necessary. In the next section, we expect that $\omega_d \to 0$ as $f \to 0$. Therefore, it is reasonable to predict that the scaling function $G_d'(u)$ with $\delta_d=0$. There is a trend for that all sets of data collapse to $\delta_d=0$ in Fig. 4(b).

In Fig. 4(c), we plot $s^{\tau_d}P_d(s,f)$ as a function of $u=sf$. Compared with Fig. 3(c) with $\Delta_a=-0.11$, $s^{\tau_d}P_d(s,f)$ has a steeper slope in the power-law region. We expect that $\Delta_d=\delta_d-\tau_d=-1$. This explains why τ_d is very different from the direct measurement exponent ω_d because Δ_d has large deviation from 0. In Table I, we list the values for D_d, τ_d, Δ_d, and δ_d. Since for each f the crossover between the power-law decay and the exponential decay is located at the same position for the sf axis shown in Fig. 4(b), we expect $s_{m2}f$ is a constant. Therefore, we can conclude that $[s_{m1},s_{m2}]=[k_{d1},k_{d2}/f]$, where k_{d1} and k_{d2} are cutoff constants for dissipative waves. Again, $[\ln(s_{f1}),\ln(s_{f2})] \approx [\ln(s_{m1}),\ln(s_{m2})]$ for $k_{d1}=4$ and $k_{d2}=0.32$.

We now turn to the probability distribution of the last waves $P_l(s,f)$. In Fig. 5(a), $P_l(s,f)$ is plotted as a function of sf. The power-law behavior is expressed as $P_l(s,f) \sim s^{-\omega_l(f)}$. We choose the fitting interval $[s_{f1},s_{f2}]=[2^2,2^3]$, $[2^2,2^6]$, $[2^2,2^{10}]$, and $[2^2,2^{13}]$ and then find $\omega_l=1.15$, 1.28, 1.31, and 1.34 for $f=10^{-2}$, 10^{-3}, 10^{-4}, and 10^{-5}, respectively. The dependence between ω_l and f shows that $\omega_l(f)$ is a monotonically decreasing function. Again, using the data $\sigma_l(1)=0.63$ and $D_l=1$ in the inset of Fig. 1, we obtain $\tau_l=2D_l-\sigma_l(1)=1.37$ and plot $f^{\sigma_l(1)-2D_l}P_l(s,f)=f^{-1.37}P_d$ as a function of $sf^{D_l}=sf$ in Fig. 5(b). For the simple scaling, we still need to consider the correction because that ω_l is not a constant in our considered range for f. In the next section, we predict that $\omega_l(f) \to 1.375$ as $f \to 0$. Therefore, we expect that $\delta_l=1.375$. In Fig. 5(c), the plot $s^{1.37}P_l$ as a function of sf is shown. From this figure, we also can expect that $\Delta_l=\delta_l-\tau_d=0.005$. In Table I, we list the values for D_l, τ_l, Δ_l, and δ_l. Furthermore, we have $[s_{m1},s_{m2}]=[k_{l1},k_{l2}/f]$, where k_{l1} and k_{l2} are cutoff constants for last waves. Again, $[\ln(s_{f1}),\ln(s_{f2})] \approx [\ln(s_{m1}),\ln(s_{m2})]$ for $k_{l1}=4$ and $k_{l2}=0.08$.

The corrections to simple scaling are necessary when ω_x is not a constant in the considered range of f. In general, if

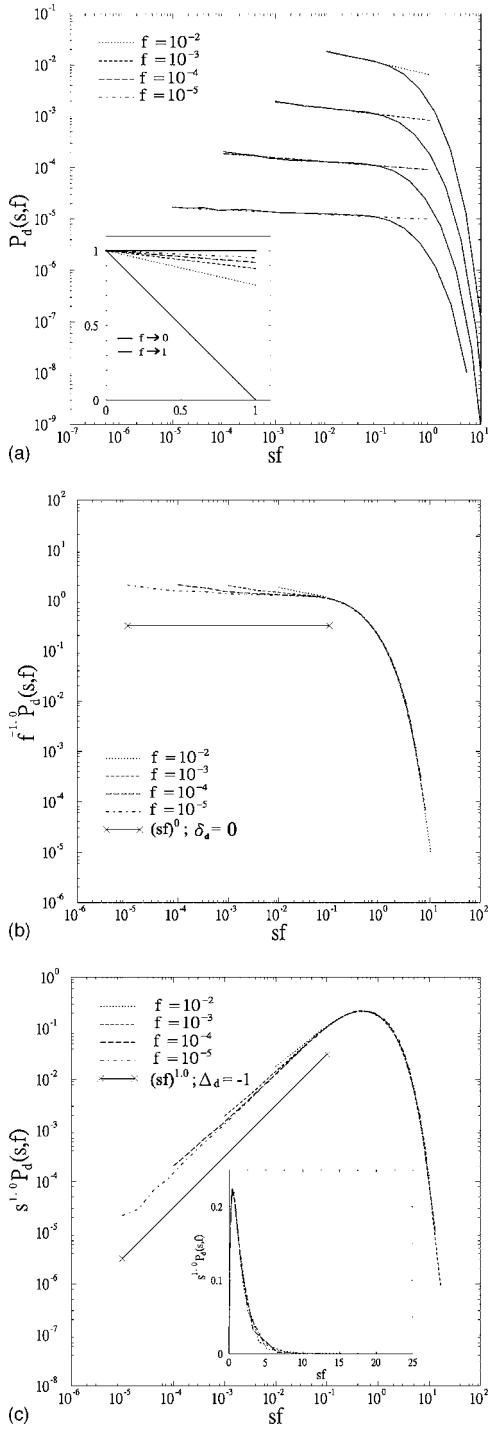

FIG. 4. (a) The probability distribution for dissipative waves $P_d(s,f)$ as a function of sf. The linear fittings of $P_d(s,f)$ are plotted as straight lines for $f=10^{-2}$ (dotted line), 10^{-3} (dash line), 10^{-4} (long dash line), and 10^{-5} (dotted dash line). The inset shows four curves with the same line types and slopes as these fitting curves of $P_d(s,f)$ for $f=10^{-2}$, 10^{-3}, 10^{-4}, and 10^{-5}, respectively. Here, we also plot two curves with slopes 0 and -1 which correspond to our predicted slopes for $P_d(s,f\to 0)$ (solid line) and $P_d(s,f\to 1)$ (thick solid line), respectively. (b) $f^{-1.0}P_d(s,f)$ as a function of sf for the data from (a). Here, we expect that $\delta_d=0$. (c) The log-log plot of $s^{1.0}P_d(s,f)$ as a function of sf for the data from (a). Here, we expect that $\Delta_d=-1.0$. The inset shows the same function in the original scale.

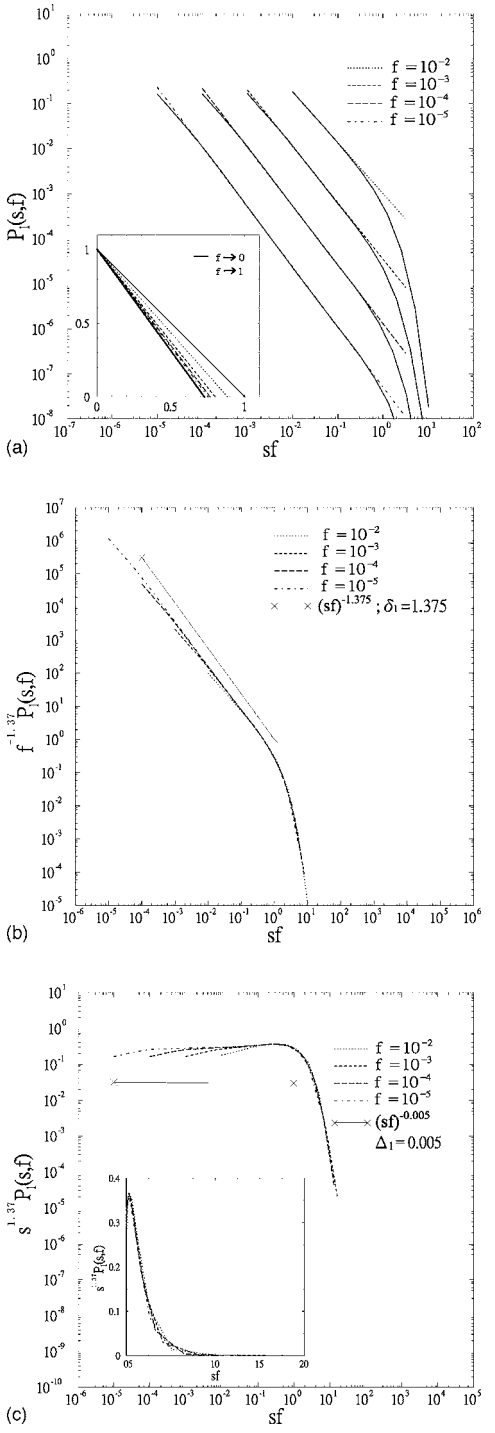

FIG. 5. (a) The probability distribution for all waves $P_l(s,f)$ as a function of sf. The linear fittings of $P_l(s,f)$ are plotted as straight lines for $f=10^{-2}$ (dotted line), 10^{-3} (dash line), 10^{-4} (long dash line), and 10^{-5} (dotted dash line). The inset shows four curves with the same line types and slopes as these fitting curves of $P_l(s,f)$ for $f=10^{-2}$, 10^{-3}, 10^{-4}, and 10^{-5}, respectively. Here, we also plot two curves with slopes $-\frac{11}{8}$ and -1 which correspond to our predicted slopes for $P_l(s,f\to 0)$ (solid line) and $P_l(s,f\to 1)$ (thick solid line), respectively. (b) $f^{-1.37}P_l(s,f)$ as a function of sf for the data from (a). Here, we expect that $\delta_l=1.375$. (c) The log-log plot of $s^{1.37}P_d(s,f)$ as a function of sf for the data from (a). Here, we expect that $\Delta_d=0.005$. The inset shows the same function in the original scale.

the correction term (or the effect of the subdominant exponents) is obvious, the equality $\sigma_x(q)=D_x(q-\tau_x+1)$ will not be exactly satisfied [23]. However, in the inset of Fig. 1, we find this equality is nicely fitted even when ω_x is not a constant for $x=d$ and l. The reason can be explained by the insets of Figs. 3(c), 4(c), and 5(c) which are the plots for $s^{\tau_x}P_x$ as a function of sf in the original scale. The scaling function $G_x(u)$ in the original scale is well approximated by these insets. Originally, $\sigma_x(q)$ shown in Eq. (9) will be well determined if the obtained values of $\int u^{q-\tau_x}G_x(u)du$ for various f are the same. However, from the obtained $G_x(u)$ for various f shown in the insets of Fig. 3(c), 4(c), and 5(c), we find that $\int u^{q-\tau_x}G_x(u)du$ are mainly contributed by the interval $[u_x^{\max},\infty]$ where $G_x(u_x^{\max})$ is the maximum of $G_x(u)$. This intervals $[0,u_x^{\max}]$ and $[u_x^{\max},\infty]$ nearly correspond to the power-law and tail parts of P_x, respectively. Therefore, the obtained D_x and τ_x are almost controlled by the tail parts. Since that tails of curves in the Figs. 4(b), 4(c), 5(b), and 5(c) are nicely collapsed, we can conclude that $\sigma_x(q)=D_x(q-\tau_x+1)$ is well satisfied.

In Ref. [11], DeMenech *et al.* reported that the BTW sandpile manifests multifractal scaling. They also pointed out two discoveries of the BTW sandpile. (1) Due to a very peculiar role played by a class of rare and large avalanche, a standard simple scaling could be effectively recovered. (2) The moment of probability distribution are fully determined by these rare and large avalanches. From their investigation and our result in the validity of $\sigma_x(q)=D_x(q-\tau_x+1)$, we expect that the rare and large waves (which correspond to the tail part of P_x) in the DT model play a critical role to maintain the simple scaling.

A wave being both dissipative and last is called a dissipative last wave. In order to understand $P_d(s,f)$ and $P_l(s,f)$, it is worth studying $P_{ld}(s,f)$, the probability distribution of dissipative last waves. We expect $P_{ld}(s,f)\sim s^{-\omega_{ld}(f)}$ in the power-law range and calculate the exponent $\omega_{ld}(f)$ of dissipative last waves. The numerical results show that $\omega_{ld}(f)\approx 0.39$ for each f. Note that ω_{ld} in the DT model is almost a constant but that the corresponding value in the BTW model is 1 [28]. This deviation of ω_{ld} between the BTW and DT models is due to the different mechanics of dissipation where BTW is boundary dissipation but DT is bulk dissipation. Finally, the values of the exponent ω_x as a function of f are plotted in Fig. 6 for $x=a$, d, l, and ld.

IV. ANALYSIS OF DIRECT MEASUREMENT EXPONENTS

Suppose that the total number of all waves for a simulation is $\mathcal{N}_a$. Therefore, $d\mathcal{N}_a$ is the number of all waves between s and $s+ds$. In the same simulation, there are $\mathcal{N}_d$ dissipative waves. For a given f at a specified wave size s, there are $4s$ times to dissipate a grain by probability f. A wave being nondissipative is in probability $(1-f)^{4s}$. Therefore, the probability of a wave being dissipative is $[1-(1-f)^{4s}]$. Then, we have that $d\mathcal{N}_d=[1-(1-f)^{4s}]d\mathcal{N}_a$. However, we have $d\mathcal{N}_a\sim P_a(s,f)ds$ and $d\mathcal{N}_d\sim P_d(s,f)ds$. Therefore, the probability distribution of dissipative wave P_d as a function of s at a given f can be expressed as follows:

$$P_d(s,f)=R_d(f)[1-(1-f)^{4s}]P_a(s,f), \tag{11}$$

where $R_d(f)$ is a normalization constant. In the power-law region $s_{m1}\le s\le s_{m2}$, we have $P_a(s,f)\sim s^{-\omega_a}$ and $P_d(s,f)\sim s^{-\omega_d(f)}$. Therefore, from Eq. (11), $s^{-\omega_d(f)}\sim[1-(1-f)^{4s}]s^{-\omega_a}$ holds only in the interval $[s_{m1},s_{m2}]$. We expect that $s_{m1}=k_{d1}$ and $s_{m2}=k_{d2}/f$, where $k_{d1}=4$ and $k_{d2}=0.32$ are from the numerical simulations on dissipative waves.

Consider the following two limitations for f. (i) $f\to 0$. For a finite s, we have $[1-(1-f)^{4s}]=4sf+\mathcal{O}(f^2)$. Therefore, we have $s^{-\omega_d(f)}\sim[1-(1-f)^{4s}]s^{-\omega_a}=(4sf)s^{-1}\sim s^0$ when $f\to 0$ and then we expect that $\omega_d(f\to 0)=0$ [29]. Compared with all waves, dissipative waves are rare when f is very small. Furthermore, for $f=0$, there is no dissipative wave, i.e., $P_d=0$. It is consistent to the conditions $s_{m2}=\infty$ and $\omega_d=0$ [29]. (ii) $f\to 1$. Alternatively, when f is close to 1, almost every toppling will dissipate grains through Eq. (2). That means $P_d\approx P_a$. One example is shown in the $f=0.1$ case of Fig. 2, where $P_d(s,f=0.1)\approx P_a(s,f=0.1)$. Therefore, we conjecture that $\omega_d(f)\approx\omega_a=1$ at $f\to 1$. The inset of Fig. 4(a) shows the fitting and predicted slopes of the power-law behavior for various f. The dependence between ω_d and f satisfies that $\omega_d(f)$ is a monotonically increasing function.

By the direct calculation of the derivative of $\ln P_d(s,f)$ versus $\ln(s)$, we obtain the measured exponent ω_{dm} for dissipative waves as a function of s and f as follows:

$$\omega_{dm}(s,f)=-\frac{d\ln P_d(s,f)}{d\ln(s)}=\omega_a+\frac{4s(1-f)^{4s}\ln(1-f)}{1-(1-f)^{4s}}. \tag{12}$$

It must be noted that s is a discrete integer quantity. However, ω_{dm} is obtained from a continuous function. Therefore, it becomes meaningless by using ω_{dm} at any specified integer s to represent ω_d. Averaging ω_{dm} over s from s_{m1} to s_{m2} may be a good approximation for ω_d. The function form of Eq. (12) illustrates that ω_{dm} approximates to a function of sf when s is large and f is small. Therefore, $\omega_{dm}(s,f)|_{s=s_{m2}}$ is a constant for each f ($s_{m2}f=k_{d2}$ is a constant here). This does not imply that ω_d is a constant since $\omega_{dm}(s,f)|_{s=s_{m1}}$ is different for each f. In addition, the probability distribution is always shown in a double logarithm plot which implies that the average should be based on $d\ln(s)$ (with weight $1/s$) but not on ds (with weight 1). Therefore, the approximate value of ω_d can be expressed as

$$\overline{\omega_{dm}}(f)=\frac{\int_{\ln(s_{m1})}^{\ln(s_{m2})}\omega_{dm}d\ln(s)}{\ln(s_{m2})-\ln(s_{m1})}=\omega_a+\frac{4\ln(1-f)}{[\ln(s_{m2})-\ln(s_{m1})]}\int_{s_{m1}}^{s_{m2}}\frac{(1-f)^{4s}}{[1-(1-f)^{4s}]}ds. \tag{13}$$

The above expression can be reduced to the mean slope of Eq. (11) between s_{m1} and s_{m2}. Finally, we obtain $\overline{\omega_{dm}}=\omega_a-\{\ln[1-(1-f)^{4s_{m2}}]-\ln[1-(1-f)^{4s_{m1}}]\}/[\ln(s_{m2})-\ln(s_{m1})]$.

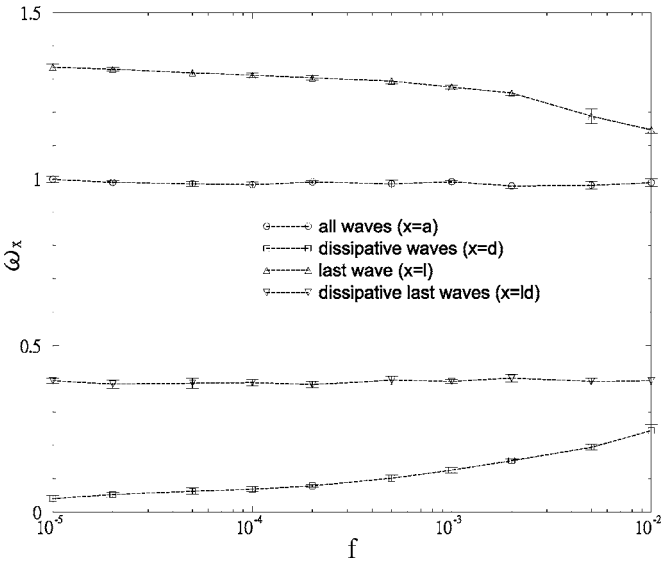

FIG. 6. The exponents of the direct measurement as a function of f for all waves ω_a (○), dissipative waves ω_d (□), last waves ω_l (△), and dissipative last waves ω_{ld} (▽).

Here, we use $s_{m1}=4$ and $s_{m2}=32$ at $f=10^{-2}$ (i.e., $k_{d1}=4$ and $k_{d2}=0.32$ from simulations). Therefore, $f=10^{-3}$, 10^{-4}, and 10^{-5} correspond to $s_{m2}=k_{d2}/f=$ 320, 3200 and 32000, respectively. This setting is consistent with the fitting interval $[s_{f1},s_{f2}]$ for P_d from simulations in the sense of a log-log plot. The expected $\overline{\omega_{dm}}(f)$ is listed in Table II, and we find that it is close to $\omega_d(f)$ from the simulations. It is interesting to note that $s_{m2}=3.2<s_{m1}=4$ at $f=0.1$ from $k_{d1}=4$ and $k_{d2}=0.32$. This contradicts that $s_{m2}>s_{m1}$ and explains why the power-law behavior is broken at $f=0.1$. Finally, we consider the deviations of $\overline{\omega_{dm}}$ for different $[s_{m1},s_{m2}]$ in the $f=10^{-5}$ (10^{-2}) case. (i) $[k_{d1},k_{d2}]=[4,0.16]$, $[4,0.32]$, and $[4,0.64]$. We obtain $\overline{\omega_{dm}}=$ 0.037 (0.162), 0.064 (0.238), and 0.105 (0.341), respectively. (ii) $[k_{d1},k_{d2}]=[2,0.32]$, $[4,0.32]$, and $[8,0.32]$. We obtain $\overline{\omega_{dm}}=$ 0.059 (0.193), 0.064 (0.238), and 0.069 (0.302), respectively. We conclude that $\overline{\omega_{dm}}(f)$ depends on the values of s_{m1} and s_{m2}, and our choice for s_{m1} and s_{m2} can satisfy the trend of $\omega_d(f)$.

In the Sec. III, we define the probability distribution of dissipative last waves $P_{ld}(s,f)$. Furthermore, we can also define the conservative last waves as the nondissipative part of the last waves. This is obtained from last waves abandoning dissipative events and retaining nondissipative events. Its probability distribution is denoted by $P_{l0}(s,f)$. In this way, the ratio of the number of conservative last waves to the number of last waves at a fixed s is $(1-f)^{4s}$. Therefore, we expect

$$P_{l0}(s,f)=R_{l0}(f)(1-f)^{4s}P_l(s,f), \tag{14}$$

where $R_{l0}(f)$ is a normalization constant. In addition, the conservative last waves of the DT model are generally similar to the last waves of the BTW model in the bulk. The exponent of the last waves in the BTW model is 11/8 [13]. Therefore, we expect that $P_{l0}\sim s^{-11/8}$ and $P_l\sim s^{-\omega_l(f)}$ in the power-law region. From Eq. (14), we have $s^{-\omega_l(f)}\sim(1-f)^{-4s}s^{-11/8}$ in the interval $s_{m1}\leq s\leq s_{m2}$.

Consider two limitations for f. (i) $f\to 0$. The DT with $L\to\infty$ and $f\to 0$ is similar to the bulk of BTW with $L\to\infty$ since the toppling rule is the same for both cases. Therefore, $\omega_l(f\to 0)=11/8$ [13], which is the value of the last waves for the BTW. This observation can be also considered by the asymptotic behavior of Eq. (14) as follows: for a finite s, $\lim_{f\to 0}(1-f)^{-4s}=\lim_{f\to 0}(1+4sf)=1$. We have that $s^{-\omega_l(f)}\sim(1-f)^{-4s}s^{-11/8}\sim s^{-11/8}$ when $f\to 0$. Therefore, $\omega_l(f\to 0)=\frac{11}{8}$. (ii) $f\to 1$. An avalanche should contain only one wave since strong dissipation terminates topplings, i.e., $P_l\approx P_a$ when $f\to 1$. Again, an example is shown in Fig. 2 where $P_l(s,f=0.1)\approx P_a(s,f=0.1)$. Therefore, $\omega_l(f\to 1)\approx\omega_a=1$. This trend is verified and can be seen in the inset of Fig. 5(a) which shows the fitting and predicted slopes of power-law behavior for various f. The dependence between ω_l and f satisfies that $\omega_l(f)$ is a monotonically decreasing function.

Repeating the procedure of deriving the exponent from $\omega_{lm}=-d\ln P_l(s)/d\ln(s)$ and then averaging ω_{lm} over s_{m1} to s_{m2} on $\ln(s)$ scale, we obtain

$$\overline{\omega_{lm}}(f)=\frac{11}{8}+\frac{4(s_{m2}-s_{m1})\ln(1-f)}{\ln(s_{m2})-\ln(s_{m1})}. \tag{15}$$

If we take $s_{m1}=k_{l1}=4$ and $s_{m2}=k_{l2}/f=0.08/f$ which are consistent with $[s_{f1},s_{f2}]$ for P_l from simulations, then the $\overline{\omega_{lm}}(f)$ will be close to the simulation result $\omega_l(f)$ listed in Table II. Again, consider the deviations of $\overline{\omega_{lm}}(f)$ for different $[s_{m1},s_{m2}]$ in the $f=10^{-5}$ (10^{-2}) case. (1) $[k_{l1},k_{l2}]=[4,0.04]$, $[4,0.08]$, and $[4,0.16]$. We obtain $\overline{\omega_{lm}}=$ 1.352 (1.214), 1.333 (1.143), and 1.298 (1.027), respectively. (2) $[k_{l1},k_{l2}]=[2,0.08]$, $[4,0.08]$, and $[8,0.08]$. We obtain $\overline{\omega_{lm}}=$ 1.336 (1.201), 1.333 (1.143), and 1.329 (1.053), respectively. We conclude that $\overline{\omega_{lm}}(f)$ depends on the values of s_{m1} and s_{m2}, and our choice for s_{m1} and s_{m2} can satisfy the trend of $\omega_l(f)$.

TABLE II. The obtained critical exponents ω_d and ω_l from numerical simulations and the expected critical exponents $\overline{\omega_{dm}}$ and $\overline{\omega_{lm}}$ for each f.

f	10^{-2}	5×10^{-3}	10^{-3}	5×10^{-4}	10^{-4}	5×10^{-5}	10^{-5}
ω_d	0.24±0.02	0.19±0.01	0.13±0.01	0.10±0.01	0.07±0.01	0.06±0.01	0.04±0.01
$\overline{\omega_{dm}}$	0.238	0.192	0.129	0.112	0.086	0.078	0.064
ω_l	1.15±0.01	1.19±0.02	1.28±0.01	1.29±0.01	1.31±0.01	1.32±0.01	1.34±0.01
$\overline{\omega_{lm}}$	1.143	1.201	1.274	1.290	1.315	1.322	1.333

In Table II, $\omega_l(f)+\omega_d(f)$ (≈ 1.39 on average) is almost a constant for each f. The mathematical formula that P_l of Eq. (14) multiplied by P_d of Eq. (11) in the power-law region can be expressed as

$$P_l(s,f)P_d(s,f) \sim \frac{[1-(1-f)^{4s}]}{(1-f)^{4s}} s^{-1} s^{-11/8} \sim s^{-[\omega_l(f)+\omega_d(f)]}. \tag{16}$$

Here, we expect that $[1-(1-f)^{4s}](1-f)^{-4s} \sim s^{\varepsilon}$ where ε is a constant in the power-law region. When f is small, we have $[1-(1-f)^{4s}](1-f)^{-4s} \sim s$. Therefore, we conjecture that $\varepsilon = 1$ and $P_l P_d \sim s s^{-1} s^{-11/8} = s^{-11/8}$, i.e., $\omega_l(f)+\omega_d(f) = \frac{11}{8} = 1.375$ which is close to our simulation. In addition, it is worth noting that $P_l P_d$ cannot be considered as P_{ld}. From the discussion of last waves, P_{ld} is proportional to $[1-(1-f)^{4s}]P_l(s,f)$. Therefore, in the power-law region we expect that

$$P_{ld}(s,f) \sim s^{-\omega_{ld}(f)} \sim [1-(1-f)^{4s}](1-f)^{-4s} s^{-11/8} \sim s^{-3/8}. \tag{17}$$

Finally, we predict that $\omega_{ld}(f) = \frac{3}{8} = 0.375$ for each f. This result is also confirmed by our numerical results with $\omega_{ld} \approx 0.39$ on average shown in Fig. 6.

V. DISCUSSION

If a probability distribution satisfies the simple scaling, it is questionable to use the direct measurement exponent (ω_x) to represent the exponent defined by the simple scaling (τ_x) [25]. First, $\omega_x(f)$ may differ from δ_x. We have that $\delta_x = \omega_x$ as $f < f_x^c$ and $\delta_x \neq \omega_x$ as $f > f_x^c$. In this paper, we find $\delta_a = \omega_a(f)$, $\delta_d \neq \omega_d(f)$, and $\delta_l \neq \omega_l(f)$ for $10^{-2} \geq f \geq 10^{-5}$. That is to say $f_a^c \geq 10^{-2}$, $f_d^c < 10^{-5}$, and $f_l^c < 10^{-5}$. Secondly, δ_x may differ from τ_x because Δ_x may not be 0. In this paper, we find three classes for the dependence between δ_x and τ_x: $\Delta_a = -0.11$ (δ_a is not far from τ_a), $\Delta_d = -1$ (δ_d is obviously different from τ_d), and $\Delta_l \approx 0$ (δ_l is very close to τ_l). In general, ω_x is easier to be obtained than τ_x. However, τ_x has much more fruitful significance than ω_x because of the simple scaling framework. On the other hand, to calculate ω_x is still helpful to understand the behavior of our system. First, the scaling function $G_x'(u)$ with exponent δ_x is directly related to ω_x. In addition, the dependence of ω_x and f is an index to observe the scaling correction.

In this paper, the obtained exponents $\omega_x(f)$ for direct measurement in the DT sandpiles are consistent with the analytic expressions. We also point out that the dissipation plays a very important role in the DT sandpile based on the following findings. (1) The simple scaling is effectively recovered by the large and rare events (the tail part of P_x) which are strongly related to small dissipation. These large and rare events shown in the insets of Figs. 3(c), 4(c), and 5(c) determine the values of σ_x. (2) The upper cutoffs s_{m2} of power-law behaviors for all, dissipative, and last waves are governed by dissipations. This is evident that s_{m2} for all, dissipative, and last waves in the DT model are all proportional to f^{-1}. However, from Fig. 1, we find that $s_d \sim f^{-1}$, $s_a \sim f^{-0.89}$, and $s_l \sim f^{-0.63}$. Therefore, dissipation is really important since the upper cutoffs s_{m2} for all, last, and dissipative waves are only proportional to s_d. Finally, our discovery of exponents may be helpful to the investigate of bulk dissipation for other SOC models, e.g., the OFC model [30].

ACKNOWLEDGMENTS

This work was supported by the National Science Council of Taiwan, R.O.C. under Grant No. NSC 93-2112-M-194-005.

[1] P. Bak, C. Tang, and K. Wiesenfeld, Phys. Rev. Lett. **59**, 381 (1987); Phys. Rev. A **38**, 364 (1988).
[2] H. E. Stanley, *Introduction to Phase Transitions and Critical Phenomena* (Oxford University Press, New York, 1971).
[3] P. Bak, *How Nature Works: The Science of Self-Organized Criticality* (Copernicus, New York, 1996).
[4] M. Alava, e-print cond-mat/0307688.
[5] S. S. Manna, J. Phys. A **24**, L363 (1991).
[6] K. Christensen, A. Corral, V. Frette, J. Feder, and T. Jøssang, Phys. Rev. Lett. **77**, 107 (1996).
[7] Z. Olami, Hans Jacob S. Feder, and K. Christensen, Phys. Rev. Lett. **68**, 1244 (1992).
[8] A. Chessa, E. Marinari, and A. Vespignani, Phys. Rev. Lett. **80**, 4217 (1998).
[9] A. Vespignani, R. Dickman, M. A. Munoz, and S. Zapperi, Phys. Rev. E **62**, 4564 (2000).
[10] B. Drossel, Phys. Rev. E **61**, R2168 (2000).
[11] M. DeMenech, A. L. Stella, and C. Tebaldi, Phys. Rev. E **58**, R2677 (1998).
[12] C. Tebaldi, M. De Menech, and A. L. Stella, Phys. Rev. Lett. **83**, 3952 (1999).
[13] D. Dhar and S. S. Manna, Phys. Rev. E **49**, 2684 (1994).
[14] E. V. Ivashkevich, D. V. Ktitarev, and V. B. Priezzhev, Physica A **209**, 347 (1994).
[15] V. B. Priezzhev, D. V. Ktitarev, and E. V. Ivashkevich, Phys. Rev. Lett. **76**, 2093 (1996).
[16] D. V. Ktitarev, S. Lübeck, P. Grassberger, and V. B. Priezzhev, Phys. Rev. E **61**, 81 (2000).
[17] D. Dhar, Phys. Rev. Lett. **64**, 1613 (1990).
[18] S. N. Majumdar and D. Dhar, Physica A **185**, 129 (1992).
[19] S. N. Majumdar and D. Dhar, J. Phys. A **24**, L357 (1991); V. B. Priezzhev, J. Stat. Phys. **74**, 955 (1994); E. V. Ivashkevich, J. Phys. A **27**, 3643 (1994).
[20] From Eq. (1), $z_I \leq 4$ after the first toppling of site I. However, it may have $z_I > 4$ during the toppling process since other sites may transfer grains to site I. In this case, we do not topple site I again (i.e., keep $z_I > 4$) but topple all other unstable sites. The height of lattice site i should arrive at $z_i \leq 4$ except $i=I$.
[21] It is straightforward to generalize this statement to that if we allow the initial site I to topple K times, every toppling site

topples at most K times. Avalanches correspond to the case $K \to \infty$. From the result of Ref. [12], we expect that the scaling behavior is better when K becomes smaller.

[22] In this paper, we focus our attention on the range of f to ensure $s_x \ll L^2$. For a given L, there exists a cutoff $f_{\min}$, which satisfies $s_x = s_x(f) \ll L^2$ for $f > f_{\min}$. When s_x is comparable to L^2, we expect that the function form should change to $s_x = s_x(L,f)$ even the periodic boundary is set.

[23] R. Pastor-Satorras and A. Vespignani, Phys. Rev. E **61**, 4854 (2000).

[24] That $\tau_x < 1$ will make the normalization condition $\int P_x ds = 1$ questionable. For more in details, see Chap. 2 of Ref. [25].

[25] G. Pruessner, Ph.D. thesis, University of London, London, 2004.

[26] L. P. Kadanoff, S. R. Nagel, L. Wu, and S. M. Zhou, Phys. Rev. A **39**, 6524 (1989).

[27] F. J. Wegner, Phys. Rev. B **5**, 4529 (1972).

[28] C.-K. Hu, E. V. Ivashkevich, C.-Y. Lin, and V. B. Priezzhev, Phys. Rev. Lett. **85**, 4048 (2000), and references therein. The exponents shown in this reference follow the definition of Eq. (6).

[29] For a finite system, s_{m2} of Eq. (6) is finite. In this case, $\int_{s_{m1}}^{s_{m2}} s^{-\omega_x} ds$ is finite for any ω_x. Therefore, $\omega_x \leq 1$ is allowed. On the other hand, s_{m2} is infinite for an infinite system. In such a case, for $\omega_x \leq 1$, $\int_{s_{m1}}^{s_{m2}} s^{-\omega_x} ds$ will be infinite. It means that the normalization constant c_x of the form $P_x = c_x s^{-\omega_x}$ should be 0. Therefore, we have $P_x = 0$ for $\omega_x \leq 1$.

[30] S. Lise and M. Paczuski, Phys. Rev. E **63**, 036111 (2001).